TM-AFM NONLINEAR MOTION CONTROL WITH ROBUSTNESS ANALYSIS TO PARAMETRIC ERRORS IN THE CONTROL SIGNAL DETERMINATION

José Manoel Balthazar

Universidade Estadual Paulista – UNESP, Rio Claro-SP, Brazil; e-mail: jmbaltha@rc.unesp.br

Angelo Marcelo Tusset

Universidade Tecnológica Federal do Paraná – UTFPR, Ponta Grossa-PR, Brazil; e-mail: a.m.tusset@gmail.com

Átila Madureira Bueno

Universidade Estadual Paulista – UNESP, Sorocaba-SP, Brazil; e-mail: atila@sorocaba.unesp.br

Nonlinear motion of the microcantilever probe in the Atomic Force Microscope (AFM) has been extensively studied considering mainly the van der Waals forces. Since the behavior of the microcantilever is vital to quality of generated images, the study of control strategies that force the probe to avoid undesired behavior such as chaotic motion, is also of significant importance. A number of published works has shown that the microcantilever is subject to chaotic motion for a certain combination of parameters. For such a parameter combination, the control system must suppress the chaotic motion. Here, an study of the AFM mathematical model is presented, aiming to find a region of operation of the AFM where the motion is chaotic. In order to suppress the chaotic motion, a periodic orbit of the system is obtained, and the controller forces the system to that periodic orbit. Two control strategies are used, namely: The State Dependent Riccati Equation (SDRE) and the Optimal Linear Feedback Control (OLFC). Both control strategies consider the complete nonlinearities of the system, and the OLFC guarantees the global stability. The numerical simulations carried out showed the efficiency of the control methods as well as the sensitivity of each control strategy to parametric errors. Without the parametric errors, both control strategies were effective in maintaining the system into the desired orbit. On the other hand, in the presence of parametric errors, the SDRE technique was more robust than the OLFC.

Key words: AFM, SDRE control, optimal linear feedback control, uncertainty

1. Introduction

The invention of the Scanning Tunneling Microscope (STM) and of the Atomic Force Microscope (AFM) by Gerd Binnig, in the 1980s, started surface investigation in the atomic scale. Since then, many improvements and developements had been made achieving important results by simple contact measurements. Nevertheless, the contact AFM cannot generate true atomic resolution in stable operation (Mestron *et al.*, 2007; Morita *et al.*, 2009; Bhushan, 2004). The AFM system has become a popular and useful instrument to measure intermolecular forces that can be applied in electronics, biological analysis, materials, semiconductors, etc.

A typical AFM consists of a microcantilever with a sharp tip mounted to a piezoelectric actuator, as shown in Fig. 1. The microcantilever displacement is determined by a position sensitive photodetector, from a laser beam reflected off the microcantilever end-point, providing feedback signal to the control system (Morita *et al.*, 2009; Bhushan, 2004; Jalili *et al.*, 2004).

In the mid 1990s, noncontact AFM techniques achived true atomic resolution under attractive regime at room temperature. The noncontact AFM operates in the static mode or dynamic mode, i.e., static AFM or dynamic AFM, respectively. In the static AFM, the force F_{ts} interacting

between the tip and sample translates into deflection of the cantilever, and the image is a map (x, y, F_{ts}) with $F_{ts} = \text{const}$.

Different techniques provide several opportunities to take pictures from different types of samples, generating a wide range of information. The different methods of generating images – also called scanning modes or modes of operation – mainly refer to the distance between the probe tip and the sample at the time of scanning, and to the ways the tip moves over the sample surface. The tip displacement due to the tip and sample interaction forces are translated into images, and since the tip and sample forces strongly depend on the tip and sample distance, different modes of operation generate different images (Frétigny, 2007; Morita *et al.*, 2009; Bueno *et al.*, 2012).

The two dinamic AFM basic methods are Amplitude Modulation (AM-AFM) and Frequency Modulation (FM-AFM), in both AM-AFM and FM-AFM the microcantilever is deliberately vibrated at a predetermined amplitude and frequency, near the microcantilever eigenfrequency. The tip-sample interaction forces cause changes in the amplitude, phase and frequency of the microcantilever oscillation, i.e., the tip-sample interaction forces are modulated in the microcantilever motion (Morita *et al.*, 2009; Bueno *et al.*, 2012; Polesel-Maris and Gauthier, 2005; Couturier *et al.*, 2001; Bueno *et al.*, 2010; Zhong *et al.*, 1993). Initially, the AM-AFM was used only in noncontact mode, but later it was also used at a closer distance involving repulsive tip-sample interactions in the intermittent contact mode AFM, or Tapping Mode (TM-AFM).

In the tapping mode, the microcantilever amplitude of oscillation is modulated as the microcantilever tip scans the sample. This modulation causes the microcantilever tip to only tap on the sample surface near the extreme of the oscillation cycle, minimizing the frictional forces that are present in the contact mode and reducing the damage on soft samples, providing high resolution topographic images even for sample surfaces that are easily damaged or dificult to image by other AFM techniques (Morita *et al.*, 2009; Zhong *et al.*, 1993; Hansma *et al.*, 1994).

Under certain physical conditions the AFM system is subject to undesirable behaviors such as bifurcations and chaotic motion, due to the nonlinear effects of the tip-sample interaction forces. This type of irregular motion impairs the AFM performance since it degrades the atomic forces measurements, generating poor resolution and inaccurate images. In the TM-AFM the chaotic motion often occur during the transition from noncontact to tapping mode indicating the presence of complex dinamics (Morita *et al.*, 2009; Bhushan, 2004; Ashhab *et al.*, 1999a; Hu and Raman, 2006; Raman *et al.*, 2008).

The nonlinear behavior of the microcantilever has also been used to improve sensitivity and material contrast by modulating high frequency distortions on the microcantilever motion when the microcantilever is harmonically driven very close to the sample surface. In principle, higher harmonics contain detailed information about the tip-sample potential (Morita *et al.*, 2009; Raman, 2008)

In the literature, a number of control methods have been proposed aiming to suppress or mitigate undesirable irregular motion and its effects. In (Yabuno, 2008), the microcantilever amplitude of vibration is controlled by applying an additional nonlinear damping via nonlinear feedback. In (Hornstein and Gottlieb, 2008), the model differs from standard lumped mass models by the inclusion of nonlinear elastic terms yielding a consistent set of system parameters that incorporates the influence of the modified microcantilever dispersion and the controller, which is introduced as a part of the generalized force, and affects both the equilibrium and the time dependent solution of the microcantilever equation.

In (Yamasue and Hikihara, 2006), a chaotic microcantilever in AM-AFM is stabilized using the Time-Delayed Feedback Control (TDFC) method, forcing the microcantilever to a periodic orbit of the system. In (Salarieh and Alasty, 2009), a chaotic TM-AFM is controlled using the TDFC method. The feedback gain is obtained and adapted according to a minimun entropy algorithm. In (Ashhab *et al.*, 1999a), the AFM is modeled considering the van der Waals potential

force, and the cantilever is vibrated by a sinusoidal input. The forced dynamics is analysed using the Melnikov method determining the regions of the parameter space in which chaotic motion is possible. Then, using a PI controller, the Melnikov method is computed again, and the obtained relation is used to suppress the chaotic motion.

In (Yamasue *et al.*, 2009), an experimental stabilization of irregular and non-periodic microcantilever oscillation in the AM-AFM with the TDFC technique is demonstrated using a magnetic excitation instead of typical piezoelectric excitation. In (Balthazar *et al.*, 2013), the TM-AFM operating in liquid is modeled, and chaotic motion is identified for a wide range of the parameter values, and two control techniques used to suppress the chaotic motion are compared, namely, the Optimal Linear Feedback Control (OLFC), proposed by Rafikov *et al.* (2008) and the TDFC, showing that the OLFC presents a faster transient response than the TDFC.

In this work, the TM-AFM operating in vacuum is modeled based on the forced dynamical system suggested by Ashhab *et al.* (1999b), and the chaotic motion is observed for a certain parameter combination. In order to suppress the microcantilever chaotic motion, two control techniques are proposed, the Optimal Linear Feedback Control (OLFC) and the State-Dependent Riccati Equation (SDRE). Additionally, the robustness of both control techniques is tested considering parameter uncertainties on the TM-AFM model and on the control signal.

In Section 2, the mathematical model of the TM-AFM is described. In Section 3, the control of chaotic motion by the application of the OLFC and SDRE methods is presented. In Section 4, the robustness of the control techniques is tested by including parameters uncertainties on the control signal determination. The final remarks and the acknowledgments are in Sections 5 and 6, respectively.

2. TM-AFM mathematical model

The physical model of the TM-AFM is shown in Fig. 1. The basis of the microcantilever is excited by a dither-piezo generating a displacement $\psi \cos(wt)$. The microcantilever is controlled by a piezo-actuator.
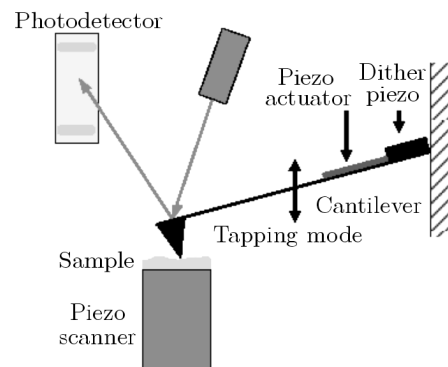

Fig. 1. Model of an AFM

The first mode of vibration of the TM-AFM microcantilever can be modeled as a vibrating mass-spring-damper system (Morita *et al.*, 2009; Bhushan, 2004; Zhang *et al.*, 2009) vibrating close to the surface of the sample, as shown in Fig. 2. The tip is considered as a sphere of radius R. In the equilibrium position (when only the gravity acts on it), the distance between the cantilever tip and the sample is given by Z_0. The position of the cantilever measured from the equilibrium position is given by x. The mass of the microcantilever is given by m, and the spring and damping coefficients are given by k and c, respectively. F_u is the control system force used to control the microcantilever displacement by means of the Piezo-actuator.
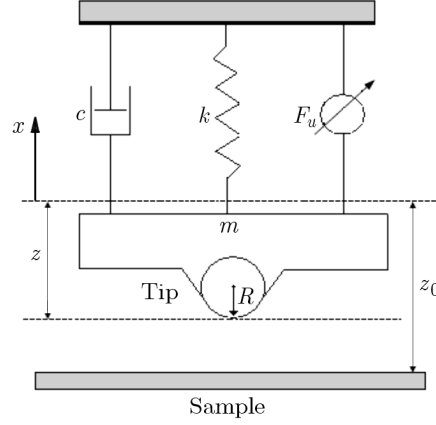
Fig. 2. Model representative of AFM through a mass-spring-damper

According to Rutzel *et al.* (2003), the interaction between the tip of the cantilever and the surface of the sample can be modeled as being the interaction between a sphere and a flat surface, as

$$U_{LJ}(x, z_0) = \frac{A_1 R}{1260(z_0 + x)^7} - \frac{A_2 R}{6(z_0 + x)} \tag{2.1}$$

where $U_{LJ}(x, z_0)$ is the Lennard-Jones (LJ) potential, A_1 and A_2 are the Hamaker constants to the attractive and repulsive potentials, respectively. Then, the potential forces are represented by a sum of the attractive and repulsive forces (van der Waals force) (Rutzel *et al.*, 2003), given by

$$F_{LJ} = -\frac{\partial U_{LJ}}{\partial(x + z_0)} = \frac{A_1 R}{180(z_0 + x)^8} - \frac{A_2 R}{6(z_0 + x)^2} \tag{2.2}$$

In the TM-AFM, the tip only touches the surface of the sample in the maximum amplitude of oscillation. The contact between the tip and the sample is complicated and delicate, this the main reason to use this operation mode in fragile samples. Since the microcantilever must be driven to periocally oscilate during the scanning process, the microcantilever is excited by a harmonic force (Ashhab *et al.*, 1999b; Yamasue and Hikihara, 2006; Salarieh and Alasty, 2009; Morita *et al.*, 2009; Giessibl, 1995)

$$F = \psi \cos wt \tag{2.3}$$

The conservative spring force is given by

$$F_k = kx \tag{2.4}$$

The dissipative force is given by:

$$F_c = c\dot{x} \tag{2.5}$$

From the equilibrium of forces acting on the microcantilever, it results that $m\ddot{x} = -F_k - F_c + F_{LJ} + F + F_u$ and considering the foregoing relations (Eqs. (2.2)-(2.5)), the governing equation of motion becomes

$$m\ddot{x} + c\dot{x} + kx = \frac{A_1 R}{180(z_0 + x)^8} - \frac{A_2 R}{6(z_0 + x)^2} + \psi \cos wt + F_u \tag{2.6}$$

Taking into account the following relationship between the variables in (2.6)

$$T = wt \qquad y = \frac{x}{z_s} \qquad \dot{y} = \frac{\dot{x}}{wz_s} \qquad w^2 = \sqrt{\frac{k}{m}}$$

$$a = \frac{z_0}{z_s} \qquad b = \frac{c}{mw} \qquad h = \frac{A_1 R}{180 mw^2 z_s^9} \qquad d = \frac{A_2 R}{6 mw^2 z_s^3}$$

$$Z_s = \frac{2}{3}\sqrt[3]{\frac{A_2 R}{3k}} \qquad U = \frac{F_u}{mw^2 z_s}$$

the dimensionless equation of motion is given by

$$y'' + by' + y - F(y) - f\cos(T) = U \tag{2.7}$$

where

$$F(x_1) = \frac{h}{(a + x_1)^8} - \frac{d}{(a + x_1)^2} \tag{2.8}$$

Defining the state variables as $x_1 = y$ and $x_2 = y'$, the dimensionless equation of motion can be transformed into state space equations, given by

$$x_1' = x_2 \qquad x_2' = -bx_2 - x_1 + F(x_1) + f\cos(T) + U \tag{2.9}$$

According to Yamasue and Hikihara (2006), Salarieh and Alasty (2009), for some parameters, the system in equation (2.9) presents chaotic behavior. Considering the parameters in Salarieh and Alasty (2009), $h = (9/25) \cdot 10^{-5}$, $f = 2$, $b = 0.04$, $d = 4/27$, $a = 0.8$. For the initial conditions $x_1(0) = 0.8$ and $x_2(0) = 0$, and for $U = 0$, the behavior of the system can be seen in Fig. 3. From the simulation results, it can be seen that the system presents chaotic behavior.

3. Chaos control in TM-AFM

Chaotic oscillations undermines the quality of the AFM images reducing the resolution and the operating range of the AFM. Stabilizing the system in a periodic orbit and suppressing the chaotic motion is essential for the accurate tip and sample interaction forces measurement (Morita *et al.*, 2009; Bueno *et al.*, 2012).

3.1. Obtaining periodic orbits

Considering the nonlinear characteristics of the van der Waals force – see Eqs. (2.2) and (2.8), in order to simplify the mathematical reasoning when applying the perturbation techniques, it is approximated by a Taylor series expansion resulting in linear quadratic and cubic terms, simplifying the mathematical reasoning. Then, from Eqs. (2.8) and (2.9), $F(y)$ is expanded in a Taylor series at the point $y = 0$, resulting

$$F(y) \approx -0.2315 + 0.5785y - 1.0839y^2 + 1.8032y^3 \tag{3.1}$$

Replacing Eq. (3.1) in Eq. (2.7) and considering $U = 0$, results

$$y'' + \varepsilon y' + c_1 y + c_2 y^2 - c_3 y^3 + p - f\cos(T) = 0 \tag{3.2}$$

where $\varepsilon = 0.04$, $c_1 = 0.4215$, $c_2 = 1.0839$, $c_3 = 1.08032$ and $p = 0.2315$.
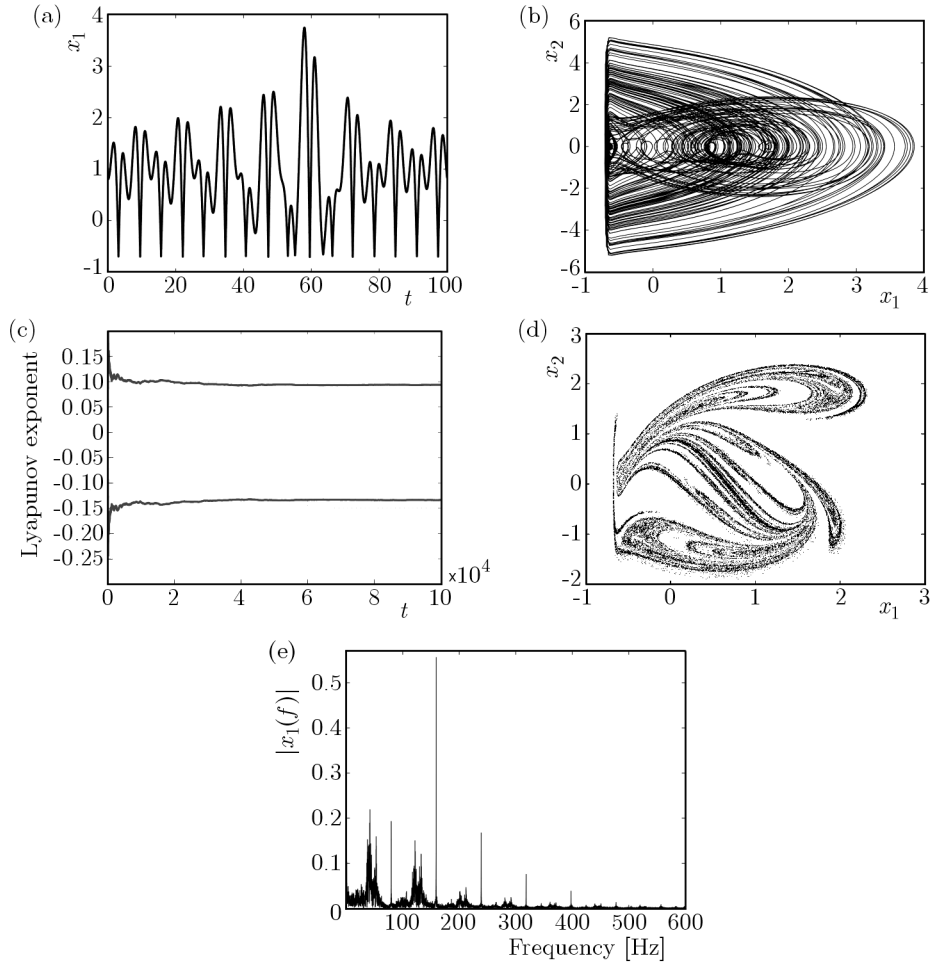
Fig. 3. (a) Microcantilever displacement; (b) phase portrait; (c) Lyapunov exponents $\lambda_1 = 0.093741$, $\lambda_2 = -0.133749$; (d) Poincaré map; (e) frequency spectrum

In order to obtain a periodic solution to Eq. (3.2), an expansion using the multiple scales method is done, considering $T_0 = T$ and $T_1 = \varepsilon T$, and solutions of the following form are looked for

$$y = \varepsilon\mu_1 + \varepsilon^2\mu_2 \tag{3.3}$$

where ε is the parameter responsible for the balance (Nayfeh, 1981), with

$$
\frac{d}{d\tau} = D_0 + \varepsilon D_1 + \varepsilon^2 D_2 + \ldots
$$
$$
\frac{d^2}{d\tau^2} = D_0^2 + 2\varepsilon D_0 D_1 + \varepsilon^2(D_1^2 + 2D_0 D_2) + \ldots \tag{3.4}
$$

then, the derivatives become

$$
D_0^2\mu_1 + c_1\mu_1 = 0
$$
$$
D_0^2\mu_2 + c_1\mu_2 = -2D_0 D_1\mu_1 - D_0\mu_1 - c_2\mu_1^2 \tag{3.5}
$$

One possible solution to the system in Eq. (3.5) is

$$y = \varepsilon a_1 \cos(\sqrt{c_1}T + \beta_1) + \varepsilon^2 a_2 \cos(\varepsilon\sqrt{c_1}T + \beta_2) + \frac{\varepsilon^2 c_2 a_1}{6c_1}\cos(2\sqrt{c_1}T + 2\beta_1) \tag{3.6}$$

For the initial conditions y_0 and y_0', it results that $\beta_1 = \beta_2 = 0$, $a_1 = y_0/\varepsilon$ and $a_2 = -y_0/(6\varepsilon c_1)$, and replacing them into Eq. (3.6) periodic orbits of the form

$$y = y_0 \cos(\sqrt{c_1}T) - \frac{\varepsilon y_0}{6c_1}\cos(\varepsilon\sqrt{c_1}T) + \frac{\varepsilon c_2 y_0}{6c_1}\cos(2\sqrt{c_1}T) \tag{3.7}$$

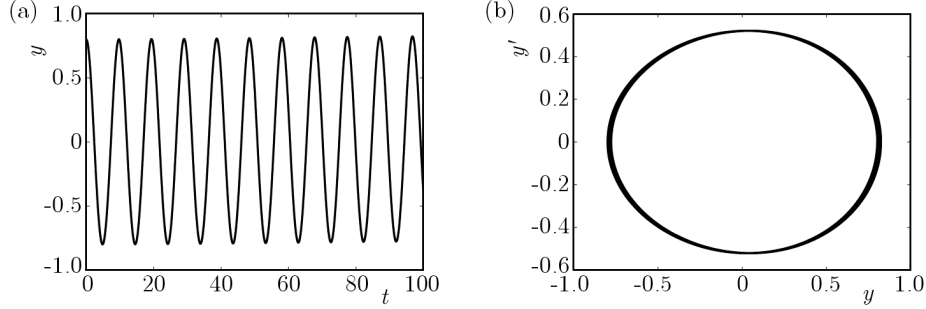are obtained. In Fig. 4, the periodic orbit for Eq. (3.7), for $y_0 = 0.8$ and $y_0' = 0$, is shown.

Fig. 4. (a) Microcantilever displacement; (b) phase portrait for solution (2.9)

3.2. Application of the OLFC

The OLFC method was developed by Rafikov *et al.* (2008). This method obtains an optimal linear feedback for a class of nonlinear systems ensuring the stability of the problem. In this section, the OLFC is applied attempting to drive the TM-AFM to the periodic orbit obtained in the previous section.

The TM-AFM equation of motion with the control law is described by the following nonlinear equation

$$x_1' = x_2 \qquad x_2' = -bx_2 - x_1 + F(x_1) + f\cos(T) + U \tag{3.8}$$

where

$$U = \widetilde{u}_o + u_{of} \tag{3.9}$$

and u_{of} is the feedback control. The feedforward optimal control $\widetilde{u}_o$ is given by

$$\widetilde{u}_o = \dot{\widetilde{x}}_2 + b\widetilde{x}_2 + \widetilde{x}_1 - F(\widetilde{x}_1) - f\cos(T) \tag{3.10}$$

where $\widetilde{\mathbf{x}}$ is the desired periodic orbit (Eq. (3.7)). Replacing Eq. (3.10) into Eq. (3.8), and defining the deviations from the desired orbit by

$$\mathbf{e} = \begin{bmatrix} e_1 \\ e_2 \end{bmatrix} = \begin{bmatrix} x_1 - \widetilde{x}_1 \\ x_2 - \widetilde{x}_2 \end{bmatrix} \tag{3.11}$$

results in

$$e_1' = e_2 \qquad e_2' = -be_2 - e_1 + F(x_1) - F(\widetilde{x}_1) + u_{of} \tag{3.12}$$

The system of Es. (3.12) is written in the following form

$$\mathbf{e}' = \mathbf{Ae} + \mathbf{G}(\mathbf{e}, \widetilde{\mathbf{x}}) + \mathbf{B}u_{of} \tag{3.13}$$

where

$$\mathbf{A} = \begin{bmatrix} 0 & 1 \\ -1 & -b \end{bmatrix} \qquad \mathbf{G}(\mathbf{e}, \widetilde{\mathbf{x}}) = \begin{bmatrix} 0 \\ F(e_1, \widetilde{x}_1) - F(\widetilde{x}_1) \end{bmatrix} \qquad \mathbf{B} = \begin{bmatrix} 0 \\ 1 \end{bmatrix}$$

According to Rafikov *et al.* (2008), Tusset *et al.* (2012b), if there exist matrices $\mathbf{Q}$ and $\mathbf{R}$ positive definite, being $\mathbf{Q}$ symmetric, such that the function

$$\widetilde{Q} = \mathbf{Q} - \mathbf{G}^{\mathrm{T}}(\mathbf{e}, \widetilde{\mathbf{x}})\mathbf{P} - \mathbf{P}\mathbf{G}(\mathbf{e}, \widetilde{\mathbf{x}}) \tag{3.14}$$

is positive definite for the bounded matrix $\mathbf{G}$, then the linear feedback control u_{of} is optimal and transfers the nonlinear systems from any initial state to the final state

$$\mathbf{e}(\infty) = \mathbf{0} \tag{3.15}$$

minimizing the functional

$$J = \int\limits_0^\infty (\mathbf{e}^{\mathrm{T}}\widetilde{\mathbf{Q}}\mathbf{e} + \mathbf{u}_{of}^{\mathrm{T}}\mathbf{R}\mathbf{u}_{of})\, dt \tag{3.16}$$

The control u_{of} can be found by solving the equation

$$u_{of} = -\mathbf{K}\mathbf{e} \tag{3.17}$$

where $\mathbf{K} = \mathbf{R}^{-1}\mathbf{B}^{\mathrm{T}}\mathbf{P}$ and the symmetric matrix $\mathbf{P}$ can be determined from the algebraic Riccati equation given by

$$\mathbf{P}\mathbf{A} + \mathbf{A}^{\mathrm{T}}\mathbf{P} - \mathbf{P}\mathbf{B}\mathbf{R}^{-1}\mathbf{B}^{\mathrm{T}}\mathbf{P} + \mathbf{Q} = \mathbf{0} \tag{3.18}$$

Defining the desired trajectory as the periodic orbit in equation (3.7), which was obtained from the Multiple Scales method, and considering the matrices $\mathbf{A}$ and $\mathbf{B}$, given by

$$\mathbf{A} = \begin{bmatrix} 0 & 1 \\ -1 & -0.04 \end{bmatrix} \qquad \mathbf{B} = \begin{bmatrix} 0 \\ 1 \end{bmatrix} \tag{3.19}$$

Choosing

$$\mathbf{Q} = 10^4 \begin{bmatrix} 1 & 0 \\ 0 & 0.1 \end{bmatrix} \qquad \mathbf{R} = [0.01] \tag{3.20}$$

and solving equation (3.18), results

$$\mathbf{P} = \begin{bmatrix} 3193.7138 & 9.99 \\ 9.99 & 3.1933 \end{bmatrix} \qquad \mathbf{K} = \begin{bmatrix} 999 & 319 \end{bmatrix} \tag{3.21}$$

Replacing equation (3.21) into equation (3.17), the optimal feedback control law is given by

$$u_{of} = -999e_1 - 319e_2 = -999(x_1 - \widetilde{x}_1) - 319(x_2 - \widetilde{x}_2) \tag{3.22}$$

For the optimal control verification, the function in equation (3.14) is numerically calculated by $L(T) = \mathbf{e}^{\mathrm{T}}\widetilde{\mathbf{Q}}\mathbf{e}$. The sufficient criterion to guarantee that the control signal in equation (3.22) is optimal is that $L(T)$ is positive definite (Rafikov *et al.*, 2008).

Figure 5 shows the application of the OLFC to the TM-AFM problem. As observed in Fig. 4b, the function $L(T)$ is positive definite for $\mathbf{e} \to \mathbf{0}$. It can be concluded that the control signal of equation (3.22) is optimal and moves the system of equation (3.8) to the desired orbit given by equation (3.7) in less than two seconds, as observed in Fig. 4a.

3.3. State-Dependent Riccati Equation (SDRE)

The SDRE strategy is an effective algorithm for synthesizing nonlinear feedback controls by allowing the nonlinearities in the system states and, additionally, offering great design flexibility through state-dependent weighting matrices (Tusset and Balthazar, 2012; Tusset *et al.*, 2012a; Mracek and Cloutier, 1998).

3.3.1. Application of SDRE control

The dynamic system defined by Eq. (2.9) can be parameterized in first order equations and written in the state-dependent coefficient (SDC) and the non state-dependent coefficient in the following way (Tusset *et al.*, 2012c)

$$\mathbf{X}' = \mathbf{A}(\mathbf{X})\mathbf{X} + \mathbf{B}U_s + \mathbf{\Phi}(\mathbf{X}, T) \tag{3.23}$$

where $\mathbf{X} = [x_1, x_2]^{\mathrm{T}}$ is the time dependent state vector and $\mathbf{X}' \in R^2$ is the derivative of the state vector. $U_s = u_{sf} + \widetilde{u}_s$, where u_{sf} is the feedback control, $\widetilde{u}_s$ is the feedforward control and $\mathbf{\Phi}(\mathbf{X}, T)$ is the nonlinearities vector. The initial and final conditions are given by $\mathbf{X}(t_0) = \mathbf{X}_0$, $\mathbf{X}(\infty) = \mathbf{0}$, respectively.
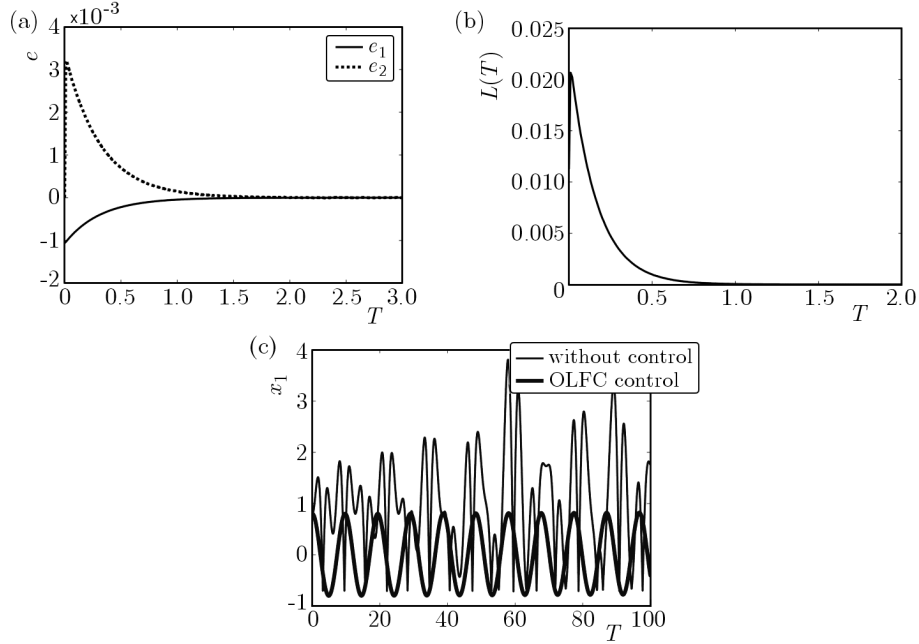

Fig. 5. (a) Deviations from the desired orbit; (b) $L(T)$ calculated in optimal trajectory; (c) displacement of TM-AFM with and without OLFC control

Considering $F(x_1)$ as the expansion

$$F(x_1) = \frac{-dx_1(6a^5 + 15a^4x_1 + 20a^3x_1^2 + 15a^2x_1^3 + 6ax_1^4 + x_1^5)}{(a + x_1)^8} - \frac{-h + da^6}{(a + x_1)^8} \tag{3.24}$$

the coefficient dependent matrices are given by

$$\mathbf{A}(x_1) = \begin{bmatrix} 0 & 1 \\ -1 - \dfrac{dx_1(6a^5 + 15a^4x_1 + 20a^3x_1^2 + 15a^2x_1^3 + 6ax_1^4 + x_1^5)}{(a + x_1)^8} & -b \end{bmatrix}$$

$$\mathbf{\Phi}(x_1, T) = \begin{bmatrix} 0 \\ -\dfrac{-h + da^6}{(a + x_1)^8} + f\cos(wT) \end{bmatrix} \qquad \mathbf{B} = \begin{bmatrix} 0 \\ 1 \end{bmatrix} \tag{3.25}$$

A state feedback instead of an output feedback is adopted to enhance the control performance. The cost function for the regulator problem is given by

$$J = \int\limits_{t_0}^{\infty} [\mathbf{X}^{\mathrm{T}}\mathbf{Q}(\mathbf{X})\mathbf{X} + \mathbf{u}_{sf}^{\mathrm{T}}\mathbf{R}(\mathbf{X})\mathbf{u}_{sf}] \, dT \tag{3.26}$$

where $\mathbf{Q}$ is semi-positive-definite matrix and $\mathbf{R}$ positive definite.

Assuming full state feedback, the control law is given by

$$u_{sf} = -\mathbf{R}^{-1}(\mathbf{X})\mathbf{B}^{\mathrm{T}}(\mathbf{X})\mathbf{P}(\mathbf{X})\mathbf{X} \tag{3.27}$$

The estate-dependent Riccati equation to obtain $\mathbf{P}(\mathbf{X})$ is given by

$$\mathbf{A}^{\mathrm{T}}(\mathbf{X})\mathbf{P}(\mathbf{X}) + \mathbf{P}(\mathbf{X})\mathbf{A}(\mathbf{X}) - \mathbf{P}(\mathbf{X})\mathbf{B}(\mathbf{X})\mathbf{R}^{-1}(\mathbf{X})\mathbf{B}^{\mathrm{T}}(\mathbf{X})\mathbf{P}(\mathbf{X}) + \mathbf{Q}(\mathbf{X}) = \mathbf{0} \tag{3.28}$$

Defining the feedforward control as

$$\widetilde{u}_s = -\Phi(x_1, T) = \frac{-h + da^6}{(a + x_1)^8} - f\cos T \tag{3.29}$$

and replacing equation (3.29) into equation (3.23), the system of equation (3.23) can be represented as in equation (3.11) in the form of deviations

$$\mathbf{e}' = \mathbf{A}\mathbf{e} + \mathbf{B}u_{sf} \tag{3.30}$$

In Fig. 6, the application of the SDRE control technique is shown considering the matrices in Eq. (3.20). As it can be observed in Fig. 6, the SDRE technique drives the system to the desired periodic orbit of equation (3.7) in less than 2 seconds (see Fig. 6a).
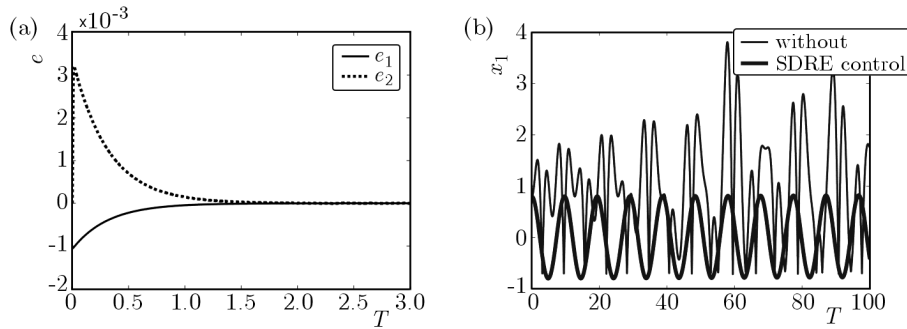

Fig. 6. (a) Deviations from the desired orbit (3.11); (b) isplacement of AFM with and without SDRE control

4. The effect of parameter uncertainties

Since mathematical models are subject to parametric inaccuracies or bad estimatives, in this Section, the robustness of the OLFC and SDRE strategies is tested considering the control signal determination sensitivity to parameter uncertainties (Shirazi *et al.*, 2011) and, in order to test the ability of controllers, the perturbed control laws are applied to the nominal dynamic system. In Section 4.1, the robustness of both control strategies is tested for parameter uncertainties in the determination of the control signal. On the other hand, in Section 4.2, the control signal determination considers the uncertainties in each parameter isolated.

4.1. Control signal determination with parameter uncertainties and measurement noise

In order to consider the effect of parameter uncertainties on the performance of the controller, the real parameters of the system are supposed to have uncertainties as follows: $\overline{f} = 1.6 + 0.8r(t)$, $\overline{b} = 0.032 + 0.016r(t)$, $a = 0.72 + 0.36r(t)$, $\overline{d} = (3.2 + 1.6r(t))/27$ and $\overline{h} = 0.288 \cdot 10^{-5} + 0.144 \cdot 10^{-5}r(t)$, where $r(t)$ are normally distributed random functions, as proposed in Shirazi *et al.* (2011). The simulation results are shown in Fig. 7.
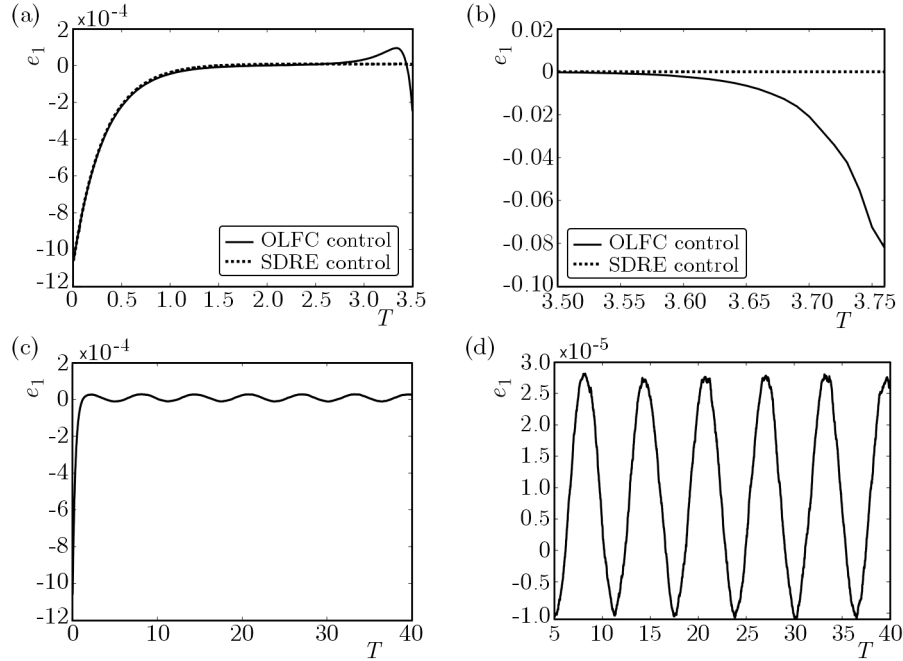

Fig. 7. Error parameters uncertainties; (a) OLFC subject to parameter uncertaintes, (b) OLFC with parameter uncetainties for $3.5 \leqslant T \leqslant 3.75$, (c) SDRE with parameter uncertainties for noise function: $0.02 \sin T$, (d) SDRE with parameter uncertainties for $5 \leqslant T \leqslant 40$ (steady state)

It can be seen in Figs. 7a and 7b that the OLFC error increase over time when the control signal determination is subject to parameters uncertainties. Additionally, Figs. 7c and 7d show the robustness of the SDRE technique when the parameters have random uncertainties and measurement noise.

4.2. Control with uncertainty

Considering that the control signal U is subject to parametric errors, the influence of each indivual parameter in the robustness of the control system is analyzed considering a random error of 20% of the nominal value. The sensitivity of the control to each parameter individually can be seen in Fig. 8. Figures 8a and 8b show that the OLFC error is unstable to uncertainties in the parameter a. In Figs. 8c and 8d, it can be seen that, except for the parameter a, the error is never larger than $2.0 \cdot 10^{-6}$. In that case, the SDRE strategy is more robust in the presence of parameter uncertainties in the control signal determination.

5. Conclusion

In order to suppress the chaotic behavior keeping the system in a controlled periodic orbit obtained from Multiple Scales method, two control strategies were considered, namely: the OLFC and SDRE strategies. Considering the results, it can be concluded that both controls are robust
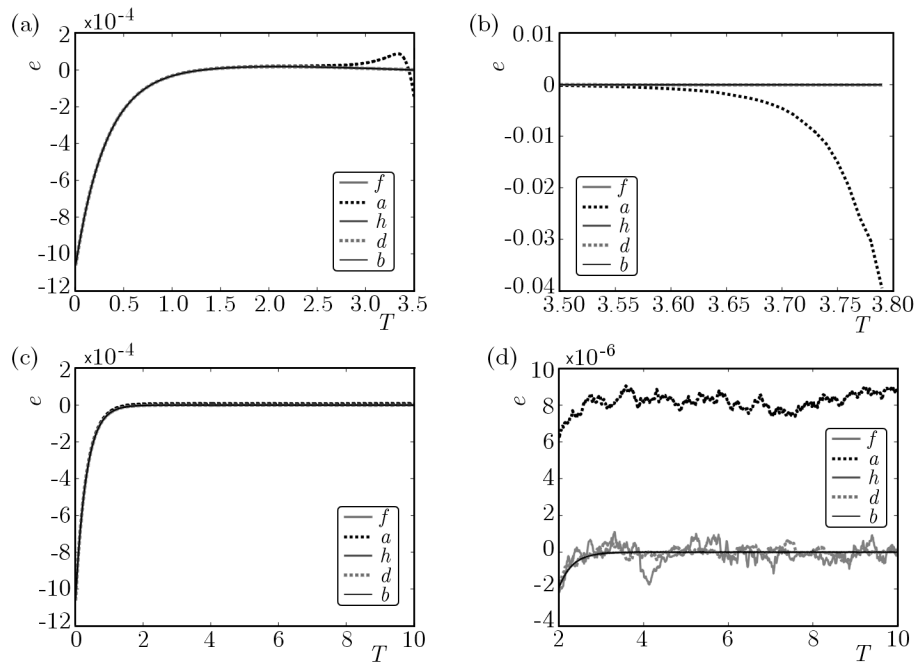
Fig. 8. Errors for individual parameter uncertainties in the control signal determination;
(a) OLFC individual parameter uncertainties, (b) OLFC individual parameter uncertainties for
$3.5 \leqslant T \leqslant 3.8$, (c) SDRE individual parameter uncertainties, (d) SDRE individual parameter
uncertainties for $2 \leqslant T \leqslant 10$

to parametric errors except for the parameter a where the error increases over time for the OLFC. Additionally, the SDRE strategy appears to have better robustness performance, even for the parameter a. The OLFC is therefore not indicated in the case of errors in the parameter a since the error becomes unstable, as shown in Figs. 7a,b, and 8a,b.

References

1. Ashhab M., Salapaka M.V., Dahleh M., Mezic I., 1999a, Dynamical analysis and control of microcantilevers, *Automatica*, **35**, 10, 1663-1670

2. Ashhab M., Salapaka M., Dahleh M., Mezić I., 1999b, Melnikov-based dynamical analysis of microcantilevers in scanning probe microscopy, *Nonlinear Dynamics*, **20**, 197-220

3. Balthazar J.M., Tusset A.M., Souza S.L.T.D., Bueno A.M., 2013, Microcantilever chaotic motion suppression in tapping mode atomic force microscope, *Proceedings of the Institution of Mechanical Engineers, Part C: Journal of Mechanical Engineering Science*, **227**, 8, 1730-1741

4. Bhushan B., 2004, *Springer Handbook of Nanotechnology*, Springer, Berlin

5. Bueno A.M., Balthazar J.M., Piqueira J.R.C., 2010, Phase-locked loop application to frequency modulation-atomic force microscope, *Proceedings of the 9th Brazilian Conference on Dynamics, Control and their Applications, DINCON 2010*, 343-348, Serra Negra, SP.

6. Bueno A.M., Balthazar J.M., Piqueira J.R.C., 2012, Phase-locked loops lock-in range in frequency modulated-atomic force microscope nonlinear control system, *Communications in Nonlinear Science and Numerical Simulation*, **17**, 7, 3101-3111

7. Couturier G., Aimé J., Salardenne J., Boisgard R., 2001, A virtual non contact-atomic force microscope (NC-AFM): Simulation and comparison with analytical models, *The European Physical Journal – Applied Physics*, **15**, 2, 141-147

8. Frétigny C., 2007, Atomic force microscopy, [In:] *Nanoscience*, Dupas C., Houdy P., Lahmani M., Editors, 91-119, Springer, Berlin, Heidelberg

9. Giessibl F., 1995, Atomic resolution of the silicon (111)-(7x7) surface by atomic force microscopy, *Science*, **267**, 5194, 68-71

10. Hansma P.K., Cleveland J.P., Radmacher M., Walters D.A., Hillner P.E., Bezanilla M., Fritz M., Vie D., Hansma H.G, Prater C.B., Massie J., Fukunaga L., Gurley J., Elings V., 1994, Tapping mode atomic force microscopy in liquids, *Applied Physics Letters*, **64**, 13, 1738-1740

11. Hornstein S., Gottlieb O., 2008, Nonlinear dynamics, stability and control of the scan process in noncontacting atomic force microscopy, *Nonlinear Dynamics*, **54**, 93-122, doi: 10.1007/s11071-008-9335-5

12. Hu S., Raman A., 2006, Chaos in atomic force microscopy, *Physical Review Letters*, **96**, 3, 036107

13. Jalili N., Dadfarnia M., Dawson D.M., 2004, A fresh insight into the microcantilever-sample interaction problem in non-contact atomic force microscopy, *Journal of Dynamic Systems, Measurement, and Control*, **126**, 2, 327-335

14. Mestrom R.M.C., Fey R.H.B., van Beek J.T.M., Phan K.L., Nijmeijer H., 2007, Modeling the dynamics of a MEMS resonator. Simulations and experiments, *Sens Actuators A*, **142**, 3, 6-15

15. Morita S., Wiesendanger R., Meyer E., Giessibl F.J., 2009, *Noncontact Atomic Force Microscopy*, Springer, Berlin

16. Mracek C.P., Cloutier J.R., 1998, Control designs for the nonlinear benchmark problem via the state-dependent riccati equation method, *International Journal of Robust and Nonlinear Control*, **8**, 4/5, 401-433

17. Nayfeh A.H., 1981, *Introduction to Perturbation Techniques*, Wiley, New York

18. Polesel-Maris J., Gauthier S., 2005, A virtual dynamic atomic force microscope for image calculations, *Journal of Applied Physics*, **97**, 4, 044902

19. Rafikov M., Balthazar J.M., Tusset A.M., 2008, An optimal linear control design for nonlinear systems, *Journal of the Brazilian Society of Mechanical Sciences and Engineering*, **30**, 12, 279-284

20. Raman A., Melcher J., Tung R., 2008, Cantilever dynamics in atomic force microscopy, *Nano Today*, **3**, 1/2, 20-27

21. Rutzel S., Lee S.I., Raman A., 2003, Nonlinear dynamics of atomic-force-microscope probes driven is Lennard-Jones potentials, *Proceedings of the Royal Society of London*, **459**, 1925-1948

22. Salarieh H., Alasty A., 2009, Control of chaos in atomic force microscopes using delayed feedback based on entropy minimization, *Communications in Nonlinear Science and Numerical Simulation*, 637-644

23. Shirazi M. J., Vatankhah R., Boroushaki M., Salarieh H., Alasty A., 2011, Application of particle swarm optimization in chaos synchronization in noisy environment in presence of unknown parameter uncertainty, *Communications in Nonlinear Science and Numerical Simulation*, **17**, 12, 742-753

24. Tusset A.M., Balthazar J.M., 2012, On the chaotic suppression of both ideal and non-ideal Duffing based vibrating systems, using a magnetorheological damper, *Differential Equations and Dynamical Systems*, 1-11, doi: 10.1007/s12591-012-0128-4

25. Tusset A.M., Balthazar J.M., Bassinello D.G., Pontes B.R., Felix J.L.P., 2012a, Statements on chaos control designs, including a fractional order dynamical system, applied to a "MEMS" comb-drive actuator, *Nonlinear Dynamics*, **69**, 4, 1837-1857, doi: 10.1007/s11071-012-0390-6

26. Tusset A.M., Balthazar J.M., Chavarette F.R, Felix J.L.P., 2012b, On energy transfer phenomena, in a nonlinear ideal and nonideal essential vibrating systems, coupled to a (MR) magneto-rheological damper, *Nonlinear Dynamics*, **69**, 4, 1859-1880, doi: 10.1007/s11071-012-0391-5

27. Tusset A.M., Balthazar J.M., Felix J.L.P., 2012c, On elimination of chaotic behavior in a non-ideal portal frame structural system, using both passive and active controls, *Journal of Vibration and Control*, 1-11, doi: 10.1177/1077546311435518

28. Yabuno H., 2008, Stabilization and utilization of nonlinear phenomena based on bifurcation control for slow dynamics, *Journal of Sound and Vibration*, 766-780.

29. Yamasue K., Hikihara T., 2006, Control of microcantilevers in dynamic force microscopy using time delayed feedback, *Review of Scientific Instruments*, 053703.1-053703.6

30. Yamasue K., Kobayashi K., Yamada H., Matsushige K., Hikihara T., 2009, Controlling chaos in dynamic-mode atomic force microscope, *Physics Letters A*, **373**, 35, 3140-3144

31. Zhang W.-M., Meng G., Zhou J.-B., Chen J.-Y., 2009, Nonlinear dynamics and chaos of microcantilever-based tm-afms with squeeze film damping effects, *Sensors*, **9**, 5, 3854-3874

32. Zhong Q., Inniss D., Kjoller K., Elings V., 1993, Fractured polymer/silica fiber surface studied by tapping mode atomic force microscopy, *Surface Science Letters*, **290**, 1/2, L688-L692